Postprint of: Prete M., Khenkin M.V., Glowienka D., Patil B.R., Lissau J.S., Dogan I., Hansen J.L., Leißner T., Fiutowski J., Rubahn H.G., Julsgaard B., Balling P., Turkovic V., Galagan Y., Katz E.A., Madsen M., Bias-Dependent Dynamics of Degradation and Recovery in Perovskite Solar Cells, ACS Applied Energy Materials, Vol. 4, No. 7 (2021), pp. 6562-6573, DOI: 10.1021/acsaem.1c00588

BIAS-DEPENDENT DYNAMICS OF DEGRADATION AND RECOVERY IN PEROVSKITE SOLAR CELLS

M. Prete[1,#], M. V. Khenkin[2,3,#], D. Glowienka[4,5#], B. R. Patil[1], J. S. Lissau[1], I. Dogan[5], J. L. Hansen[6], T. Leißner[1], J. Fiutowski[1], H.-G. Rubahn[1], B. Julsgaard[6], P. Balling[6], V. Turkovic[1], Y. Galagan[7], E. A. Katz[2]* and M. Madsen[1,]*

1. SDU NanoSYD, Mads Clausen Institute, University of Southern Denmark, Alsion 2, DK-6400 Sønderborg, Denmark
2. Dept. of Solar Energy and Environmental Physics, Swiss Inst. for Dryland Environmental and Energy Research, J. Blaustein Institutes for Desert Research, Ben-Gurion University of the Negev, Midreshet Ben-Gurion 8499000, Israel
3. Helmholtz-Zentrum Berlin für Materialien und Energie GmbH, PVcomB, Berlin, Germany
4. Faculty of Applied Physics and Mathematics, Gdańsk University of Technology, Narutowicza 11/12, 80-233 Gdańsk, Poland
5. TNO partner of Solliance, High Tech Campus 21, 5656 AE, Eindhoven, the Netherlands
6. Department of Physics and Astronomy/Interdisciplinary Nanoscience Center (iNano), Aarhus University, Ny Munkegade 120, DK-8000 Aarhus C, Denmark
7. Department of Materials Science and Engineering, National Taiwan University, Taipei 10617, Taiwan

Abstract

Degradation of perovskite solar cells (PSC) is often found to be partially or fully reversible when the cells are allowed to recover in the dark. Unlike the dynamics of degradation, knowledge about the dynamics of PSC cell recovery is very limited. Here we demonstrate that PSC recovery strongly depends on the electrical bias conditions during the light-induced degradation, and that it can be manipulated by applying external electrical bias during the recovery phase. Investigation of the recovery dynamics allow us to analyze the degradation mechanisms in detail. More specifically, we aged mixed-cation mixed-halide PSC with n-i-p structure under illumination in open circuit (OC) or short circuit (SC) conditions, and periodically measured their characteristics during the recovery. PSC aged in SC degrade faster and fully recover after the light is switched off, while the performance of cells aged in OC does not recover but instead further decreases after the light is switched off ("drop-in-dark" effect). With the use of transient photoluminescence, secondary ion mass spectrometry, and drift-diffusion based simulations, we hypothesize that extrinsic ion migration causes the drop-in-dark effect, by forming an electron extraction barrier at the metal oxide electron transport layer. The applied bias alleviates this effect. Our results are relevant for gaining a deeper understanding of the multiple degradation mechanisms present in perovskite solar cells, and for finding a practical way to assist their recovery.

Keywords: perovskite solar cells, stability and lifetime, recovery dynamics, ion migration, degradation mechanisms

Introduction

Perovskite solar cells (PSC) have radically changed the area of thin-film photovoltaics (PV), delivering rapidly increased power conversion efficiencies (PCE) during the past decade. With above 25 % PCE, the performance levels are today getting close to those of silicon PV[1]. The stability of PSC, however, possesses several challenges related to both the active perovskite layer itself and the surrounding interlayers, which are challenged by an interplay of intrinsic and extrinsic degradation effects. Degradation of the active perovskite layer under influence of external stresses such as light[2], heat[3,4] and oxygen[5,6] has been demonstrated in the past. Light illumination supports ion formation and migration[7], as well as phase segregation[8] in the active perovskite layer, resulting in both reversible and irreversible degradation mechanisms. Elevated temperatures accelerates the degradation reactions, and some PSC also undergo phase transitions at elevated temperatures, even at rather low temperatures relevant for PV applications[9]. Not only the active layer, but also the interlayers may degrade upon similar stresses. Organic interlayers, also well-known within organic PV (OPV), may degrade photo-chemically by exposure to light and oxygen[10,11], and metal oxide contact layers may form defect states[12] or an unstable interface to the active perovskite layer[13] during light exposure, leading to additional degradation. Thus, in order to keep track of and, ideally, mitigate degradation mechanisms occurring in perovskite solar cells, specific testing protocols should be applied and used to identify both the origin and type of degradation. For the same reason, the ISOS stability protocols, which were initially developed for OPV as a standard for assessing and reporting OPV stability[14], were in 2020 updated to include protocols that take into account the degradation routes that are specific for perovskite photovoltaics[15]. This includes protocols that focus on light-dark cycling (ISOS-LC) and electrical bias (ISOS-V) testing.

The light-dark cycling tests, ISOS-LC, were developed to account for reversible degradation mechanisms, which have been studied by several groups in the field of perovskite PV[16–21]. These mechanisms include: (1) light-induced formation of bulk nonradiative recombination centers, leading to large drops in the short-circuit current densities (J_{sc})[16]; (2) intrinsic ion migration, demonstrating e.g. that halide and cation vacancies migrate at different timescales, and that both can be accompanied by a full performance recovery of the cells[7,17]; (3) reversible decomposition of perovskite (self-healing effect)[18]. In a recent study, we demonstrated how a full PSC recovery, within one day-night cycle, could be seen for early stages of photo-degradation, while at more severe degradation stages, a full recovery would not take place during a time period corresponding to a one night[19]. In the same study the “drop-in-dark effect” was reported, i.e. a performance drop of the cells during the dark part of the cycle following the light-induced degradation[19]. Although the origin of this effect was not accounted for, it was revealed that it depends on the stage of the light-degradation, namely that the drop-in-dark effect can be observed only when the performance of devices decreases below at least ~60 % of the initial performance[19]. This effect of course also strongly affects the recovery dynamics of the cells.

Research strategies towards the improvement of operational stability of the PV materials and devices exhibiting (at least partially) reversible degradation may include both mitigation of the degradation mechanisms and promotion of the recovery process. Most of the published studies on perovskite PV follow the former strategies. Knowledge about attempts to promote the recovery of perovskite PV is rather absent than limited[22]. At the same time, the strategy on promoting recovery was successfully demonstrated for OPV by applying simple electrical treatment (short pulses of the reverse bias)[23,24]. Since, at least in part, the PSC degradation is due to migration of mobile ionic species, it is likely that the recovery time of PSC could be manipulated by an electrical bias as well.

In this study, we demonstrate for the first time the bias-dependent dynamics of degradation *and recovery* of perovskite solar cells. To gain a deeper understanding of the relationship between the degradation and recovery mechanisms, we investigate the PV performance at different stages of the device degradation and recovery under different electrical bias conditions. These novel investigations allow us to demonstrate that the "drop-in-dark effect" occurs only under open circuit (OC) condition, and that in some cases it can be fully mitigated by the applied electrical bias, which thus promotes faster PSC recovery. Furthermore, by utilizing a combination of characterization techniques such as transient photoluminescence (trPL) and secondary ion mass spectrometry (SIMS), in addition to drift-diffusion based device simulations, we demonstrate that the drop-in-dark effect likely occurs due to an interaction between the metal oxide defects, formed at the metal oxide surface during light degradation, and the external ions migrated from the hole transport layer during the light degradation.

More specifically, encapsulated perovskite solar cells with a layer stack structure of ITO/SnO_2/$Cs_{0.15}(CH(NH_2)_2)_{0.85}PbI_{2.7}Br_{0.3}$/Spiro-OMeTAD/Au were degraded under light until they reached 80 % or 60 % of their initial performance (T_{80} or T_{60}, respectively). In order to achieve different directions of ion migration, the cells were aged at OC and short circuit (SC) conditions. The measurements were conducted under ISOS-L-1 and ISOS-L-2 conditions[15], which correspond to 1-sun light soaking tests performed at ambient (ISOS-L-1) or elevated (ISOS-L-2) temperature, and ambient relative humidity. Following photodegradation, the dark recovery was tracked over time. To gain further insights about the degradation mechanisms, we have performed drift-diffusion based device modelling[25] to simulate experimental J(V) curves, conducted TOF-SIMS to probe ion migration, and performed transient photoluminescence (tr-PL) measurements to investigate recombination effects, at different stages of degradation and recovery. Finally, to affect the dynamics of the recovery process, and from that understand in more details the degradation mechanisms, we have for each condition applied a 30 minutes electrical bias of 0 V (reference cells), +0.5 V and -0.5 V just following the light degradation. These new studies allows us not only, for the first time, to propose a hypothesis for the origin of the "drop-in-dark effect", but the findings also point out that recovery processes, and thus also the perovskite solar cell lifetimes, can indeed be manipulated by the external electric field due to forced ions rearrangement.

Results and discussion

When comparing light-induced degradation at SC and OC conditions down to the T_{80} value (1 sun, room temperature; ISOS-L-1), we observed only a marginal difference in the degradation and recovery kinetics (see figure S1). In both cases, the decrease in PCE was quickly recovered after switching the light off. This dynamic is mainly governed by the fill factor (FF) behavior, with some contributions from the short-circuit current density (J_{sc}) and open-circuit voltage (V_{oc}).

The difference between bias conditions becomes more apparent at a later degradation stage. Figure 1 shows the comparison of photo-degradation down to T_{60} at OC and SC conditions (1 sun at an elevated temperature of 65°C, ISOS-L-2). At SC condition, the large internal electric field leads to pronounced ion migration[17,26] , which is further enhanced by the elevated temperature[17,27,28], thus explaining the difference between the rate of degradation for the two conditions. The enhanced degradation at SC condition is causing mainly large drops in FF and J_{sc}. Although the PSC degradation at OC and SC might appear similar with only a difference in the degradation rate, the recovery trends demonstrate a clear difference for significantly degraded cells. This strongly indicates that the degradation mechanisms responsible for degradation in these two cases are different. The cells degraded at SC show full recovery, while OC cells show no recovery within a 22 h period.

Instead, following light degradation in OC condition, we observe a pronounced “drop-in-dark”, which is reflected mainly in a large further decrease of FF, and appearance of s-shape characteristics in the first J(V) curve measured 1.5h after the light degradation is finished (figure 2). This is consistent with our previously reported results for OC degradation of this type of devices[19], and it is not observed for the cells degraded under SC conditions.

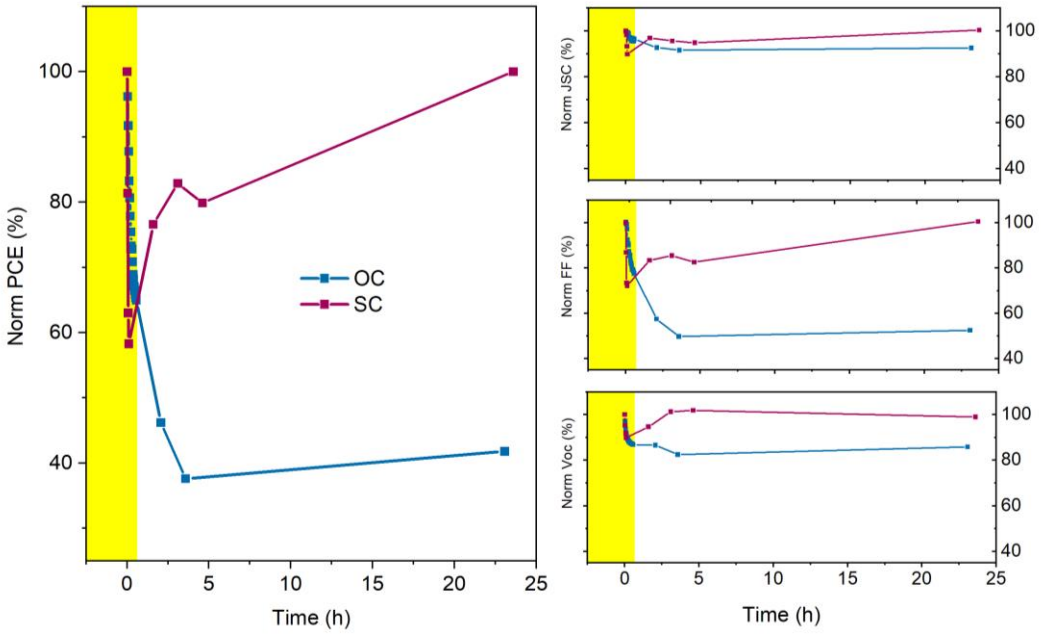

Figure 1. Time evolution of normalized principal photovoltaic parameters of the PSC during their aging under ISOS-L-2 condition (1 sun, elevated T) in OC and SC and subsequent recovery in dark. The illumination period (marked in yellow in the figures) was stopped when the cell efficiency reached ~60 % of its initial value (T_{60}).

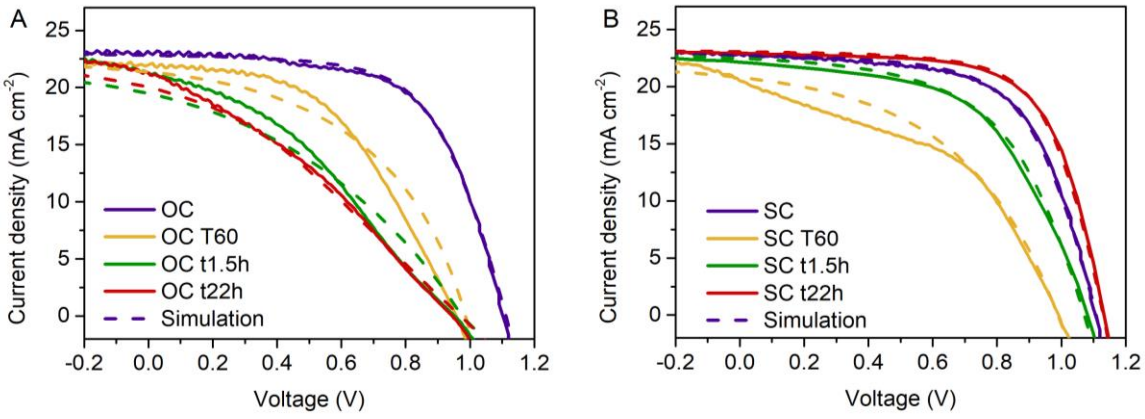

Figure 2. J(V) characteristics of fresh perovskite solar cell devices, and devices aged in OC (a) and SC (b) to T_{60} under ISOS-L-2 conditions, and then recovered in dark for 1.5 h and 22 h. Dashed lines show the drift-diffusion based simulation results.

To gain further insights into the degradation mechanisms, we have performed device simulations at several stages of the degradation-recovery experiments based on a drift-diffusion model, which quantitatively describes the generation, transport and recombination of charge carriers in the perovskite solar cell stack. In our case, the most important parameters to vary, in order to achieve a good agreement between measured and simulated J(V) curves at different stages of degradation-recovery experiments, are defect densities in the bulk and at the interfaces between perovskite and transport layers. Such defects act as recombination

sites at the respective location. Furthermore, the results of degradation-recovery experiments demonstrated it difficult to satisfactorily fit the measured J(V) curves without varying the acceptor doping concentration in the Spiro-OMeTAD hole transport layer, which mostly affects cell series resistance. Thus, these are the parameters extracted from the drift-diffusion model. We have employed this model for: 1) fresh solar cells, 2) solar cells degraded to either T_{80} or T_{60}, and 3, 4) solar cells recovered for 1.5 hours and 22 hours in dark after light degradation, i.e. t1.5h and t22h, respectively, see figure 2. The parameter values obtained from the drift-diffusion based simulations at the different stages of degradation and recovery are shown in Table 1. Also, based on the step value of each parameter, the equivalent error of the extracted parameter is calculated to be lower than 10%. For the T_{80} case, the experimentally measured results and corresponding drift-diffusion simulation are shown in figures S2. As some of the parameters employed in the model have similar effects on the J(V) curves measured at 1 sun, we found it useful to employ experimentally obtained light intensity dependent J(V) curves to increase the reliability of the model. These are shown in figure S3. We note that all initial cell paramteres are liste in table S1.

Table 1. Parameter output of drift-diffusion simulation of J(V) curves for cells degraded to T_{60} in OC and SC conditions, and recovered over 22 hours (t1.5h and t22h). For parameters where the values are calculated for holes and electrons separately, the values for holes are provided in brackets.

OC without bias	**Unit**	**t_0**	**T_{60}**	**t1.5h**	**t22h**
Acceptor doping concentration	m^{-3}	1,00E+23	1,10E+23	6,00E+22	8,50E+21
Series resistance	$\Omega\ cm^{-2}$	4	1	10	10
Defect density at SnO_2 interface	m^{-2}	1,00E+14	2,00E+16	2,00E+16	4,00E+15
Bulk defect density	m^{-3}	3,00E+21 (3,00E+21)	1,00E+22 (1,00E+22)	1,50E+22 (1,50E+22)	4,00E+21 (1,00E+21)
Defect density at Spiro-OMeTAD interface	m^{-2}	(2,00E+15)	(1,00E+16)	(1,00E+16)	(1,00E+16)
SC without bias					
Acceptor doping concentration	m^{-3}	1,05E+23	1,05E+23	1,05E+23	1,10E+23
Series resistance	$\Omega\ cm^{-2}$	3	3	3	2
Defect density at SnO_2 interface	m^{-2}	1,00E+14	1,00E+16	4,00E+15	1,00E+14
Bulk defect density	m^{-3}	4,00E+21 (4,00E+21)	2,00E+22 (2,00E+22)	6,00E+21 (6,00E+21)	2,50E+21 (2,50E+21)
Defect density at Spiro-OMeTAD interface	m^{-2}	(2,00E+15)	(1,00E+16)	(1,00E+15)	(1,00E+14)

Reversible degradation mechanisms can be explained by the presence of bulk defects in the perovskite layer, for example arising from light-induced generation of bulk non-radiative recombination centers[16] and light-induced ion migration within the perovskite layer[17]. As demonstrated in the literature, the former would be more pronounced at OC conditions, where charge carriers are not extracted from the cells during light degradation, and the latter would be more pronounced at SC conditions, where the internal field is larger, supporting ions redistribution within perovskite and between the layers[27]. The modelling results show that, in our case, the average bulk defect density is slightly higher after the light degradation in the SC case, and in fact obtained in much shorter time than in the OC case (Table 1). Though an increase in the bulk defect density in our model can arise from both of the above mechanisms, i.e. it does not differentiate one from the other, the higher bulk defect density obtained in shorter times for the SC case indicates a difference in degradation mechanisms dominating under the SC and OC conditions, respectively. Based on the above-mentioned literature studies, we believe that ion redistribution is dominant for the SC case, in contrast to the OC. This can be expected due to the stronger built-in field, and the elevated temperatures which would enhance this process. We note that examples from literature have reported on faster degradation under OC

conditions compared to both MPP and SC conditions, however, studied at lower temperatures (i.e. under room temperature)[28,29].

In terms of interface degradation, our modeling results demonstrate larger defect densities at the SnO_2 interface upon light degradation for the OC condition, i.e. reaching a higher absolute value compared to the SC case. This is accompanied by a very minor increase in acceptor doping concentration in the Spiro-OMeTAD layer (both T_{80} and T_{60} results). We note that ion migration does take place in OC conditions, however in opposite direction than under SC, i.e. cations (and halide vacancies) migrate in OC conditions towards the electron transport layer[30,31] while anions are pushed towards the hole transport layer. Such differences in ion migration may play an important role for interface-related degradation mechanisms taking place, as observed from our modelling results, and this may be a key in understanding the different recovery behavior observed for the OC and SC light degradation conditions (figure 1). Of course, differences in the formation of trap states under OC and SC conditions may also affect the difference seen in interface-related degradation for the two conditions.

To further examine the formation/dissipation of trap states as one of the underlying mechanisms of the perovskite solar cell degradation/recovery, we involve transient photoluminescence (trPL) measurements before and after the photodegradation, as well as during the recovery in the dark. We note that these trPL measurements are conducted alongside the J(V) measurements, i.e. on the same devices and measurement series as those presented in figure 1 and 2, for the different stages of degradation and recovery. As can be seen in figure 3, photodegradation in either bias condition leads to a decrease in charge-carrier lifetime, here extracted as a weighted average lifetime[32] possibly due to an increased number of trap states, and consequently an increased rate of non-radiative recombination. During storage in the dark, in both OC and SC cases, the trPL lifetime recovers back, possibly due to a decrease in the trap density, corresponding to the recovery of the bulk defect density in our modelling results. This trend fully complies with PCE degradation-recovery for cells aged at SC but contradicts the trend of the PCE recovery curve for the cell degraded at OC, which further decreases after the light is turned off. This contradiction between PCE and trPL lifetime points out that there is a different reason for the PCE drop-in-dark effect. We acknowledge, however, that trPL lifetime measured on the full solar cell device stack, as it is performed here, might require a more complex interpretation as compared to the active material only, which is so far the main configuration for trPL studies of PSC in the literature[32] and should be a topic of further investigation. This is due to the effect of processes other than radiative or non-radiative recombination, for example, charge extraction.

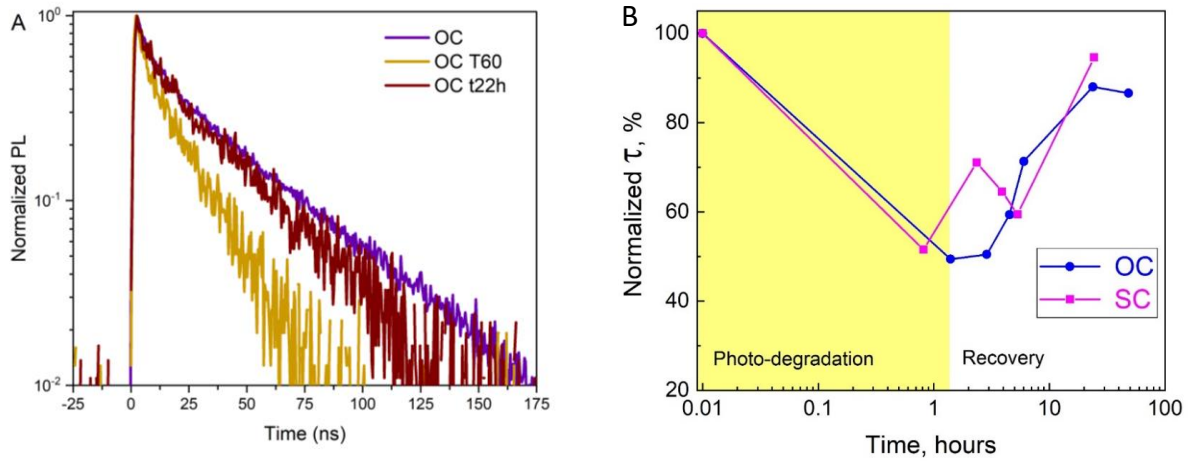

Figure 3. A) Transient PL lifetimes measured on a fresh PSC cell, after aging the cell under ISOS-L-2 condition (1 sun, elevated T) in OC condition to its T_{60} value, and after 22 h of additional recovery in dark. B) The evolution of PSC transient PL lifetime of the PSC during

their aging under ISOS-L-2 condition (1 sun, elevated T) in OC and SC and subsequent recovery in dark. The illumination period (marked in yellow in the figure) was stopped when the cell efficiency reached ~60% (corresponds to Fig.1) of its initial value.

The results of drift-diffusion simulation also demonstrate that recovery of bulk non-radiative recombination centers takes place in both OC and SC conditions, but at a slower rate in OC. As shown in Table 1, during the initial recovery phase, the OC reference cells show a drastic drop in the acceptor doping concentration in the Spiro-OMeTAD layer, which leads to an increase of the series resistance, again in contrast to the SC condition. Notably, and in strong contrast to the SC case, the electron and hole transport layer interfaces maintain a high defect density even after 22h of recovery in the OC reference case. The interface between the perovskite and electron transport SnO_2 layer seems to play a key role here, as the trap density stays approximately 50 times higher when comparing to the fresh state (Table 1). We, therefore, propose that defects at that metal oxide interface are also responsible for the "drop-in-dark" effect observed in the recovery phase of the OC conditioned cells (figure 1). Metal oxide surface defects, possibly generated during light degradation, can support the trapping of cations that migrate to the electron transport layer during photo-degradation. As demonstrated extensively in the past, metal oxides possess surface defects that can e.g. lead to physisorption or chemisorption of molecular species, which can also result in the reversible generation of trap states within the band gap of the metal oxide, for example by depletion of electrons at the oxide surface[33]. In organic solar cells, the presence of such electron traps at the surface of metal oxides is well-known to lead to pronounced s-shape J(V) characteristics, arising from upwards band-bending at the surface of the oxides[34] causing an extraction barrier[34]. Light soaking may lead to neutralization of such traps[35,36], and recovery of the PV parameters, mainly FF.

Surface defects formed during light degradation could thus be exposed to molecular/ionic species migrating towards that interface, which in OC conditions would likely be cations migration/accumulation at the electron transport layer. During photo-degradation, neutralization of such trapped states by light exposure can take place[35], but trapped states could cause upwards band bending at the metal oxide interface after the light is turned off, which would explain the observed s-shape characteristics at t1.5h for the OC condition (figure 2). The neutralization of the surface traps could be caused by following light-soaking, as also seen in our previous reported results[19].

To further prove the hypothesis that trapped ionic species at the surface of the metal oxide electron transport layer are responsible for the "drop-in-dark" effect, we turn towards TOF SIMS measurements to probe ion migration in the PSC stacks. To enable SIMS measurements, a batch of non-encapsulated PSC was prepared. The results of degradation-recovery experiments with these samples are qualitatively similar to those shown in Figure 1. Particularly, we see from SIMS results that gold migrates into the perovskite layer through the Spiro-OMeTAD layer, under both SC and OC degradation conditions, although more severely under SC conditions (Figure 4b). This has also been demonstrated as an irreversible degradation mechanism in other studies in the past[37]. Unexpectedly, lithium ions were observed all across the PSC also for the fresh cell; however, a further redistribution of the lithium ions is seen upon degradation at SC and OC conditions. We note that in a separate experiment, we checked that the SIMS process itself, i.e. the material removal by sputtering, did not cause the lithium ions to distribute across the device layer stack (figure S4). The lithium ion concentration near the electron transport interface is largest following OC degradation, indicating lithium ion migration towards and trapping at the SnO_2 interface for OC-aged cells. It should be noted that the SIMS measurements are taken many hours following the actual light-degradation, and such a shift in lithium ion concentration could likely mean little or no back-migration of ions following light degradation, i.e. trapping of lithium ions at the SnO_2 interface. Lithium ion migration in perovskite solar cells has been demonstrated in the past, also reaching the metal oxide electron transport layer as shown here, causing severe hysteresis effects[38]. Based on the presented TOF SIMS results, the apparent trapped states at the SnO_2 layer/perovskite

interface found from drift-diffusion based simulations could be assumed to arise from lithium ions trapped at that interface. Recent work also demonstrates lithium ion insertion in SnO_2 to form intermediate phases of Li_xSnO_2[39], however, further studies would be required to determine the nature of the trapped ionic species here. Alternatively, oxygen adsorption and desorption could cause this effect, as previously demonstrated for TiO_x interlayers[35], where depletion of electrons at the surface of the oxide would cause band bending and energetic offsets leading to the s-shape characteristics seen here. To further support the assumptions of ion-induced trapped states at the SnO_2 layers causing the drop-in-dark effect, the J(V) curve at t1.5h recovery of the OC-aged cells (drop-in-dark curve) where simulated again including band bending at the interface of the oxide layer (figure S5). Indeed, the simulations capture the s-shape characteristics observed experimentally, providing a better fit when band bending at the SnO_2 layer is included.

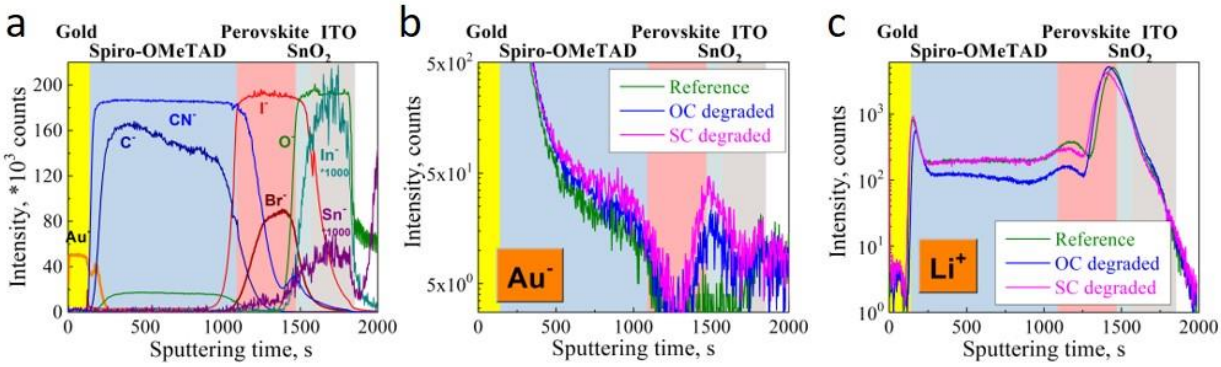

Figure 4. a) Elements disctribution in TOF-SIMS depth profile for fresh PSC, b,c) depth profiles for Au (b) and Li (c) ions in fresh devices and those degraded under OC condition to ~T50 or SC to ~T30 (1 sun, elevated T, non-encapsulated).

The mechanisms described above significantly depend on the drift of mobile charges inside the devices. It is, therefore, reasonable to suggest that the application of a short-term electrical bias during the recovery might help to speed up or slow down the recovery depending on the electric field direction. Figure 5 shows the recovery of perovskite solar cells degraded at OC and SC conditions to T_{60}, without and with applying ±0.5 V electrical bias during the first 30 minutes of recovery.

As already noted above, the dynamics of recovery, in particular upon applied negative bias in OC conditions, depends significantly on the precise state of degradation. For perovskite solar cells it might be sensitive to batch-to-batch and sample-to-sample variations, especially around the degradation level where the drop-in-dark effect appears[19]. We, therefore, show in Figure 5 the examples of cells with a pronounced effect and those where it only begins to develop. Independently of how pronounced the observed “drop-in-dark” effect was (figure 5a and 5b), a short negative bias application resulted in the accelerated recovery of OC-degraded PSC. This is due to significant restoration in V_{OC} and FF compared to the reference cell that was always disconnected in the dark (figure S6). It is even more interesting, considering that negative bias of the same duration and magnitude applied to a fresh cell leads to pronounced degradation of its FF (figure S7). Notably, if applied with the correct timing, a negative bias can fully mitigate the drop-in-dark effect, e.g. the reference OC results shown in Figure 5b show a drop in FF in the first dark cycle following light degradation, which is mitigated by the negative bias, figure S6. Given the above hypothesis, this may appear due to trap release in the electron transport layer by repulsion of cations (or halide vacancies) from that interface, and thus recovering of the band bending and removal of the s-shape characteristics. The modeling supports this hypothesis by showing a decrease in defect density at the SnO_2 interface within the first 1.5h of recovery when a negative bias is applied, which is in contrast to the reference cells (table 1), and also a faster recovery of the bulk defect density with an applied negative bias (table 2). This is further supported by the lack of s-

shape characteristics upon applied negative bias, pointing at the recovery of the interface defects at the SnO_2 layer. The fact that the FF only partially recovers, and that some J_{sc} degradation is now observed, could indicate another effect coming into play during negative biasing. If the surface defect formation in the metal oxide layer is assisted by an oxygen release, such mechanisms may include oxygen-generated degradation in the perovskite layer. Alternatively, or in addition, the formation of superoxide radical anions, a well-known contribution to irreversible degradation, may arise by electron transfer processes from SnO_2[40–42]. This may be supported by an applied positive bias, which from the simulations also show a further increase in bulk defect states that are not recovering even after t22h (Table 2). The defects at the Spiro-OMeTAD are recovering at a much slower rate, which could be explained by the lack of repelling cations back into the perovskite layer, which is otherwise supported by the applied negative bias in the OC condition. We note that while hysteresis has not been discussed in this work, it has in the past been linked to ion migration effects in perovskite cells[43,44], and thus should be observed with different magnitudes, for the cells degraded to different stages. This is shown in figure S8, demonstrating only little hysteresis effect for fresh cells, and severe hysteresis for degradaded cells.

Table 2. Parameter output of drift-diffusion based simulation of J(V) curves for cells degraded to T60 in OC and SC conditions, and recovered over 22 hours (t1.5h and t22h) following an applied bias of -0.5 V and +0.5 V for 30 min. For parameters were the values are calculated for holes and electrons separately, the values for holes are provided in brackets.

OC -0.5V bias	**Unit**	**t_0**	**T_{60}**	**t1.5h**	**t22h**
Acceptor doping concentration	m^{-3}	1,00E+23	1,20E+23	1,05E+23	1,00E+23
Series resistance	$\Omega\ cm^{-2}$	4	1	3	4
Defect density at SnO_2 interface	m^{-2}	5,00E+14	2,00E+16	1,80E+16	9,00E+15
Bulk defect density	m^{-3}	4,00E+21 (4,00E+21)	2,50E+22 (2,50E+22)	7,00E+21 (7,00E+21)	3,00E+21 (3,00E+21)
Defect density at Spiro-OMeTAD interface	m^{-2}	(2,00E+15)	(3,00E+16)	(1,00E+16)	(1,00E+15)
OC +0.5V bias					
Acceptor doping concentration	m^{-3}	1,10E+23	1,20E+23	1,00E+23	9,00E+22
Series resistance	$\Omega\ cm^{-2}$	6	1	4	6
Defect density at SnO_2 interface	m^{-2}	5,00E+14	3,00E+16	2,00E+16	1,00E+16
Bulk defect density	m^{-3}	1,30E+21 (1,30E+21)	1,00E+22 (1,00E+22)	7,00E+22 (7,00E+22)	7,00E+22 (7,00E+22)
Defect density at Spiro-OMeTAD interface	m^{-2}	(1,00E+14)	(3,00E+16)	(3,00E+16)	(1,00E+16)
SC -0.5V bias					
Acceptor doping concentration	m^{-3}	1,05E+23	1,10E+23	1,10E+23	1,00E+23
Series resistance	$\Omega\ cm^{-2}$	3	1	1	4
Defect density at SnO_2 interface	m^{-2}	1,00E+14	1,00E+16	3,60E+15	1,00E+15
Bulk defect density	m^{-3}	3,00E+21 (3,00E+21)	2,00E+22 (2,00E+22)	1,70E+22 (1,70E+22)	1,70E+22 (1,70E+22)
Defect density at Spiro-OMeTAD interface	m^{-2}	(1,00E+14)	(1,00E+16)	(1,00E+16)	(1,00E+15)
SC +0.5V bias					
Acceptor doping concentration	m^{-3}	1,05E+23	1,05E+23	1,05E+23	1,10E+23
Series resistance	$\Omega\ cm^{-2}$	3	3	3	2
Defect density at SnO_2 interface	m^{-2}	1,00E+14	1,00E+16	3,00E+15	1,00E+14
Bulk defect density	m^{-3}	4,00E+21 (4,00E+21)	2,00E+22 (2,00E+22)	2,00E+22 (2,00E+22)	3,00E+21 (3,00E+21)
Defect density at Spiro-OMeTAD interface	m^{-2}	(2,00E+15)	(1,00E+16)	(1,00E+16)	(4,00E+14)

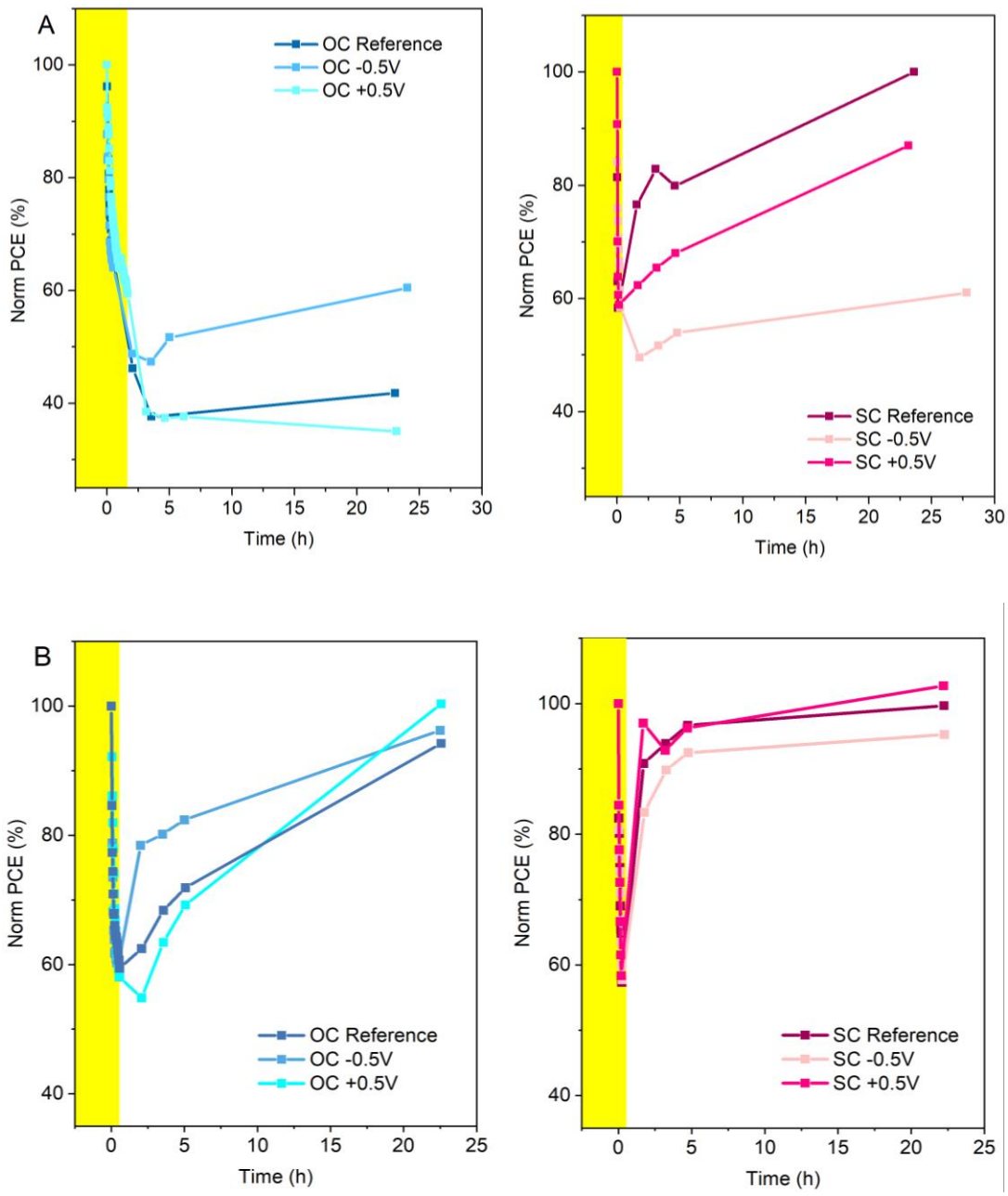

Figure 5. Time evolution of PSC PCE during their aging under ISOS-L-2 conditions in OC and SC and subsequent recovery in dark without or with an applied bias of ±0.5 V during the first 30 minutes in the dark in case of (a) strong further degradation in the dark or (b) almost no further degradation in the dark (FF drops in dark, see figure S6). The illumination was stopped when the cell efficiency reached 60 % of its initial value (T_{60}).

For the recovery from SC condition, applying a positive bias following light degradation should support ion back-migration, but as full recovery is occurring also without bias (supported by the simulations, see Table 2), this is not observed. In fact, the applied bias seems to lead to a slowed-down recovery of defect densities at the Spiro-OMeTAD interface. According to simulation results, the most important process for the recovery from the SC degradation is the large decrease of trap concentration at the SnO_2 interface, which is in strong contrast to the OC conditions. Thus, either the metal oxide defects are not formed in SC conditions, or the reverse migration direction of ions does not result in similar electron traps at that interface. The latter is in

fact supported by SIMS results in Figure 4, demonstrating a higher relative concentration of positive lithium ions at the electron transport layer in the OC condition, supporting further the proposed drop-in-dark mechanism put forward in this study. When applying a negative bias in the recovery phase of the SC cells, the bulk defect density is not recovering (Table 2), indicating that the negative bias as anticipated is slowing down the backward migration of ions from the hole transport layer interface.

Conclusions

Bias-dependent dynamics of degradation and recovery of perovskite solar cells were investigated. Perovskite solar cells degraded under ISOS-L-2 conditions show a faster degradation rate at SC conditions compared to OC conditions, due to an enhanced ion migration at elevated temperatures. During the recovery of these cells, a pronounced qualitative difference between OC- and SC-aged cells is seen, as full recovery is observed in SC condition, whereas almost no recovery is seen in OC condition. Instead, a clear drop-in-dark effect is observed in OC condition.

Using SIMS and transient photoluminescence measurements along with drift-diffusion based device simulations, we propose here that the drop-in-dark effect, observed in OC-aged cells, originates at the interface between the SnO_2 electron transport layer and perovskite active layer, demonstrating largely increased interface defect densities upon the degradation. The defects are likely a result of combined SnO_2 defect states and lithium ion migration, both taking place during light degradation of the perovskite cells in OC conditions. The ion accumulation in the SnO_2 layer forms a depletion zone with upwards band bending and s-shaped J(V) device characteristics. This is supported by the device simulations.

By investigating the bias-dependent dynamics of the recovery mechanisms following light degradation, we demonstrate that an applied negative bias can lead to trap release in the SnO_2 electron transport layer, and full recovery of the observed drop-in-dark effect. For the perovskite cells degraded under OC conditions, this leads to a significantly improved cell recovery. We note that this effect may even be improved further by fine-tuning of the bias amplitude and duration.

Keeping in mind that different underlying mechanisms are responsible for the cell degradation under SC and OC conditions, one can suggest that their combination would govern the cell aging at the maximum power point (MPP)[27,28]. This will need further experimental clarification. However, even based on the reported results one can make an important practical conclusion: the PSC degradation appears to be fully reversible at the early stages of the device aging, but becomes non-reversible (or very slowly reversible) at the later ones. From this practical point of view, having a method to prevent significant ion accumulation might help to keep the device in the "fully reversible stage" under operational conditions. For example, timely applied electrical biasing might be an effective strategy to avoid the critical accumulation of charges in the device and, thus, potentially improve both the device power output and long-term stability. Such electrical "therapy"[22] of degraded perovskite solar cells is possible and necessary to be developed.

Experimental section

Materials & Device fabrication

Perovskite solar cell devices used in this study were manufactured on 3x3 cm^2 glass substrates and contain 4 devices with an area of 16 mm^2 per substrate. The n-i-p solar cells with following device

stack were fabricated: glass/ITO/SnO_2-nps/$Cs_{0.05}(CH(NH_2)_2)_{0.79}(CH_3NH_3)_{0.16}PbI_{2.7}Br_{0.3}$/Spiro-OMeTAD/Au.

Glass substrates of 3x3 cm^2 with patterned ITO electrodes were purchased from Naranjo. The substrates were cleaned by sequential sonication in a detergent solution, deionized water, and isopropanol. The substrates were then treated with UV ozone for 30 min. Tin oxide (SnO_2) nanoparticle solution (15 wt%) purchased from Alfa Aesar was diluted by ultrapure water in a volume ratio of 1:5. Spin coating of SnO_2 solution on glass/ITO substrates was performed with a spin speed of 2800 rpm for 50 s and annealed for 30 min at 150 °C. The resulting thickness of the SnO_2 layer was 30–40 nm. After the preparation of SnO_2, samples were transferred to a N_2-filled glove box for perovskite deposition.

The perovskite precursor solution was prepared by dissolving 570.2 mg of lead iodide (PbI2) (TCI), 180.7 mg of formadiniun iodide (FAI) (GreatCell Solar), 23.8 mg methylammonium bromide (MABr) (GreatCell Solar), 34.2 mg of lead bromide ($PbBr_2$) (TCI), and 17.3 mg of cesium iodide (CsI) (Sigma Aldrich) in 0.9 mL of dimethyl formamide (DMF) and 0.1 mL of dimethyl sulfoxide (DMSO). The solution was stirred overnight at room temperature. The resulting solution was spin coated onto SnO_2-coated substrate at 2000 rpm (acceleration of 200 rpm/s) for 10 s followed by 5000 rpm (acceleration of 2000 rpm/s) for 30 s. During spin coating, 170 µL of antisolvent (chlorobenzene) was dropped onto substrate 20 s prior to the end of the program. Samples were transferred to a hotplate for annealing at 100°C for 30 min, resulting in a perovskite layer of 600 nm.

The 2,2',7,7'-tetrakis-(N,N-di-4-methoxyphenylamino)-9,9'-spirofluorine (Spiro-OMeTAD) solution (80 mg of Spiro-OMeTAD (Lumtec), 28 µL of 4-tert-butylpyridine, 17.5 µL of a 520 mg/mL $LiN(CF_3SO_2)2N$ solution in acetonitrile, and 20 µL of a 500 mg/mL FK209 cobalt salt in acetonitrile were added to 1 mL of chlorobenzene) was spin coated in air at 2000 rpm for 60 s onto the perovskite film and resulted in the formation of a 200 nm-thick hole-transporting layer. The complete Spiro-OMeTAD oxygen doping was attained by exposing the substrates to air under controlled humidity (RH 48%) for additional 30 min.

Subsequently, the substrates were transferred to the thermal evaporator under the pressure of $1.0x10^{-6}$ mbar, where 100 nm of Au back electrode was deposited on top of the Spiro-OMeTAD film. During the Au evaporation, a shadow mask was placed on each substrate, where the overlap between the ITO and Au electrodes determined the active device area of 0.16 cm^2. Encapsulation of the devices was performed by lamination of the barrier film (R2R manufactured at Holst Centre) with a pressure sensitive adhesive. The edges of the substrate were kept clean by applying a PDMS stamping route before coating each layer (and additionally cleaned where necessary) from the materials to ensure proper adhesion of the barrier film to the glass substrate at the edge and thereby prevent delamination and slow down the side ingress of water and oxygen.

Simulations

For the simulation of the PV stack, the drift–diffusion model is used. It quantitatively describes the generation, transport and recombination mechanisms with the use of the continuous equations for electrons and holes

$$\frac{\partial n}{\partial t} = G - R + \frac{1}{q}\nabla \cdot J_n, \qquad \frac{\partial p}{\partial t} = G - R - \frac{1}{q}\nabla \cdot J_p,$$

where n and p are electron and hole concentrations, respectively, q represents elementary charge constant, G is light-dependent generation rate of charge carriers and R represents the recombination processes which includes Shockley-Read-Hall, modified Langevin and Auger models. J_n and J_p are electron and hole drift-diffusion currents, respectively. The continuous equations are linked with the Poisson equation which is used to calculate the spatial distribution of the electric field

$$\nabla \cdot F = \frac{q}{\varepsilon_0 \varepsilon_r}(p - n + N_D - N_A),$$

where F represents an electric field distribution, ε_0 is vacuum permittivity and ε_r represents the dielectric constant of the material. The model has been discretized with Scharfetter-Gummel method using Chebyshev polynomials for the spatial grid and solved by forward iteration in time to find steady-state current for each applied voltage. To study the full perovskite solar cell stack, we have used the method of generalized potentials not to neglect energy differences between transporting and perovskite layer. A more detailed description of the model is given in our previous work[25].

Table 3 Parameters used in simulation of PSC. For parameters where the values are calculated for holes and electrons separately, the values for holes are provided in brackets.

	Name	Unit	SnO_2	3C perovskite	Spiro-OMeTAD
L	Thickness	nm	35	600	200
ε_r	Permittivity		9.86	24.1	2.54
$\mu_{n(p)}$	Mobility	$cm^2\ V^{-1}\ s^{-1}$	240	2 (1)	$(5.22*10^{-4})$
$C_{n(p)}$	Capturing rate	$10^{-14}\ m^3\ s^{-1}$	-	1 (1)	-
N_t	Trap density	m^{-3}	-	Variable	-
$\Gamma_{n(p)}$	Auger constant	$10^{-40}\ m^6\ s^{-1}$	-	1.55 (1.55)	-
ξ	Langevin constant		-	$1.7*10^{-5}$	-
$E_{c(v)}$	Energy level	eV	-4.00 (-8.00)	-3.88 (-5.46)	-2.40 (-5.40)
$N_{D(A)}$	Doping concentration	m^{-3}	10^{20}	$9*10^{20}$	(variable)
$N_{c(v)}$	Effective density of states	m^{-3}	$2.5*10^{25}$	$2*10^{24}$	$2.5*10^{25}$
R_s	Series resistance	$\Omega\ cm^2$	Variable		
R_{sh}	Shunt resistance	$\Omega\ cm^2$	$2*10^6$		

Table 3 shows all the parameters used for the simulation of PSC except the variables that we change for fitting the experimental data. The generation profile is calculated using the optical transfer-matrix model. Here, we have considered only the steady-state conditions and do not study the dynamical effect of ions which results in hysteresis. We have already shown that ions in steady-state conditions affect the operation of solar cells negligibly[45]. Therefore, to simplify the model and reduce the computational time we have neglected ions in dynamical form. Instead, we have made the assumption that ions acts as deep recombination centers, thus the trap concentration in general is partially related to ion concentration[46]. In our work, this assumption is used for bulk and interface trap densities. Also, the other assumption is that during the migration of ions we observe the de-doping process of Spiro-OMeTAD which results in a change of acceptor concentration level. This has a direct impact on the series resistance of the cell which we change inversely proportional to acceptor doping concentration. The other parameters are kept constant and mostly based on literature or fitting process. The SnO_2 material is used as an electron transporting layer and the electrical

parameters are adopted from literature[47,48], also the optical real and imaginary refractive index[49]. The perovskite material is defined as an active layer with electrical parameters taken from the literature[50] or from fitting to experimental data[25]. Spiro-OMeTAD material has well defined electrical[51] and optical[52] properties.

Device electrical characterization

Current-voltage, J(V), characteristics were recorded in air, applying a voltage sweep from -0.5 V to 1.5 V (forward and reverse scan directions) using a Keithley 2400 source meter and a class AAA solar simulator (Sun 3000, Abet Technologies Inc., USA) calibrated to an intensity of 1 sun (1 kW/m^2). J(V) measurements were also recorded at lower sun intensities by applying Neutral Density (ND) filters of OD1 and OD3 directly on the measured devices, achieving a light illumination intensity of 0.1 and 0.001 sun, respectively.

Device stability characterization

The device stability data were collected under accelerated conditions, measuring the photovoltaics characteristics every minute according to the ISOS-L-1 and ISOS-L-2 degradation protocol standards[12]. For the ISOS-L-2 measurements, the cells were continuously illuminated in air at 65 °C, while for the ISOS-L-1 protocol the temperature was controlled via a home-built setup at 25 °C. All the devices were characterized under the light intensity of 1 sun (AM1.5G, ISOSun InfinityPV) using a Keithley 2602A source-meter connected to a Keithley 3706A multiplexer unit, all controlled by a home-built Labview software. In this work, both open circuit (OC) and short circuit (SC) conditions were applied during aging in between measurements. After degradation, the devices were left in air at room temperature in dark to recover. During the dark recovery, reference cells are under open circuit condition, while in some of the experiments, a bias of +0.5 V or -0.5 V was applied to the devices for 30 minutes using a Keithley 2400 source meter. In all cases the total recovery time was 22 hours.

Transient Photoluminescence (trPL)

The TR-PL measurements were obtained using a streak scope (Hammatsu C106027) coupled to a custom-built laser scanning microscope (LSM), resulting in two-dimensional images, containing time-encoded spectral photoluminescence information. A commercial frequency converter (APE, HarmoniXX) attached to a sub-100 fs, 75 MHz, Ti:sapphire laser (Spectra Physics, Tsunami) was used to generate excitation beam centered at 395 nm. A pulse picker (APE, Pulse Select) furthermore decreases the repetition rate by the factor of 20. A spectrometer (Princeton Instruments SpectraPro SP-2300 with a diffraction grating 50 grooves/mm and blaze 600 nm), was used to pick up the PL signal from the samples. We finally image the resulting streak scope signal by an air-cooled CCD camera (Hamamatsu 9300). The laser scanning area was selected to ∼100 µm × 100 µm. More information can be found in our previous works[53–55]. The lifetime was deducted from a bi-exponential fit to the data. The stated lifetime is the amplitude-weighted average lifetime of the decay components, normalized to the lifetime of the fresh sample.

Secondary Ion Mass Spectrometry (SIMS)

SIMS measurements were performed using a TOF.SIMS 5 system with two ion guns and a time-of-flight mass analyzer. Probing was perfomed by 25 kV Bi-atoms at a current of 1 pA. Sputtering was performed by 3 kV Cs-atoms and a current of 30 nA. The probing area was 100 x 100 µm and the

sputter area was 200 x 200 µm. Measurements were run in interlaced mode with 20 µsec for probing and 80 µsec for sputtering.

Acknowledgments

M.M. acknowledges 'Danmarks Frie Forskningsfond, DFF FTP for funding of the project React-PV, No. 8022-00389B. V.T. and M.M. thank 'Villum Foundation' for funding of the project CompliantPV, under project number 13365. This work was supported by a research grant (17677) from VILLUM FONDEN. M.V.K. and E.A.K. acknowledge the support from the SNaPSHoTs project in the framework of the German- Israeli bilateral R&D cooperation in the feld of applied nanotechnology fundedby the German Federal Ministry for Education and Research (BMBF) and the National Technological Innovation Authority of the State of Israel. Y.G. acknowledges the Ministry of Science and Technology of Taiwan (MOST) for funding the project with the number 110-2222-E-002-001-MY3. D.G. and I.D. acknowledge the support of Solliance, a partnership of R&D organizations from the Netherlands, Belgium, and Germany working in thin film photovoltaic solar energy. All authors acknowledge support via the COST action StableNextSol, MP1307. The Numerical part has been supported by National Science Centre, Poland 2018/29/N/ST7/02326. Calculations were carried out at the Academic Computer Centre (CI TASK) in Gdansk.

Supporting information

See additional supplemental material information about all T_{80} lifetime results including device modelling, including light-intensity dependent performance parameters, dark biasing results, and modelled band bending for the T_{60} recovery J(V) curves.

Corresponding Author

* Corresponding authors: keugene@bgu.ac.il; madsen@mci.sdu.dk

[#] These authors contributed equally.

References

(1) National Renewable Energy Laboratory. Perovskite Efficiency Chart. *National Renewable Energy Laboratory*. 2019.

(2) Roose, B.; Baena, J. P. C.; Gödel, K. C.; Graetzel, M.; Hagfeldt, A.; Steiner, U.; Abate, A. Mesoporous SnO2 Electron Selective Contact Enables UV-Stable Perovskite Solar Cells. *Nano Energy* **2016**. https://doi.org/10.1016/j.nanoen.2016.10.055.

(3) Divitini, G.; Cacovich, S.; Matteocci, F.; Cinà, L.; Di Carlo, A.; Ducati, C. In Situ Observation of Heat-Induced Degradation of Perovskite Solar Cells. *Nature Energy*. 2016. https://doi.org/10.1038/NENERGY.2015.12.

(4) Juarez-Perez, E. J.; Hawash, Z.; Raga, S. R.; Ono, L. K.; Qi, Y. Thermal Degradation of CH3NH3PbI3 Perovskite into NH3 and CH3I Gases Observed by Coupled Thermogravimetry-Mass Spectrometry Analysis. *Energy*

Environ. Sci. **2016**. https://doi.org/10.1039/c6ee02016j.

(5) Bryant, D.; Aristidou, N.; Pont, S.; Sanchez-Molina, I.; Chotchunangatchaval, T.; Wheeler, S.; Durrant, J. R.; Haque, S. A. Light and Oxygen Induced Degradation Limits the Operational Stability of Methylammonium Lead Triiodide Perovskite Solar Cells. *Energy Environ. Sci.* **2016**. https://doi.org/10.1039/c6ee00409a.

(6) Aristidou, N.; Eames, C.; Sanchez-Molina, I.; Bu, X.; Kosco, J.; Saiful Islam, M.; Haque, S. A. Fast Oxygen Diffusion and Iodide Defects Mediate Oxygen-Induced Degradation of Perovskite Solar Cells. *Nat. Commun.* **2017**. https://doi.org/10.1038/ncomms15218.

(7) Xiao, Z.; Yuan, Y.; Shao, Y.; Wang, Q.; Dong, Q.; Bi, C.; Sharma, P.; Gruverman, A.; Huang, J. Giant Switchable Photovoltaic Effect in Organometal Trihalide Perovskite Devices. *Nat. Mater.* **2015**. https://doi.org/10.1038/nmat4150.

(8) Hoke, E. T.; Slotcavage, D. J.; Dohner, E. R.; Bowring, A. R.; Karunadasa, H. I.; McGehee, M. D. Reversible Photo-Induced Trap Formation in Mixed-Halide Hybrid Perovskites for Photovoltaics. *Chem. Sci.* **2015**. https://doi.org/10.1039/c4sc03141e.

(9) Röhm, H.; Leonhard, T.; Schulz, A. D.; Wagner, S.; Hoffmann, M. J.; Colsmann, A. Ferroelectric Properties of Perovskite Thin Films and Their Implications for Solar Energy Conversion. *Adv. Mater.* **2019**. https://doi.org/10.1002/adma.201806661.

(10) Sanchez, R. S.; Mas-Marza, E. Light-Induced Effects on Spiro-OMeTAD Films and Hybrid Lead Halide Perovskite Solar Cells. *Sol. Energy Mater. Sol. Cells* **2016**. https://doi.org/10.1016/j.solmat.2016.03.024.

(11) Kim, S.; Bae, S.; Lee, S. W.; Cho, K.; Lee, K. D.; Kim, H.; Park, S.; Kwon, G.; Ahn, S. W.; Lee, H. M.; Kang, Y.; Lee, H. S.; Kim, D. Relationship between Ion Migration and Interfacial Degradation of CH3NH3PbI3 Perovskite Solar Cells under Thermal Conditions. *Sci. Rep.* **2017**. https://doi.org/10.1038/s41598-017-00866-6.

(12) Ahmadpour, M.; Fernandes Cauduro, A. L.; Méthivier, C.; Kunert, B.; Labanti, C.; Resel, R.; Turkovic, V.; Rubahn, H. G.; Witkowski, N.; Schmid, A. K.; Madsen, M. Crystalline Molybdenum Oxide Layers as Efficient and Stable Hole Contacts in Organic Photovoltaic Devices. *ACS Appl. Energy Mater.* **2019**, *2*, 420–427. https://doi.org/10.1021/acsaem.8b01452.

(13) Boldyreva, A. G.; Akbulatov, A. F.; Elnaggar, M.; Luchkin, S. Y.; Danilov, A. V.; Zhidkov, I. S.; Yamilova, O. R.; Fedotov, Y. S.; Bredikhin, S. I.; Kurmaev, E. Z.; Stevenson, K. J.; Troshin, P. A. Impact of Charge Transport Layers on the Photochemical Stability of MAPbI3 in Thin Films and Perovskite Solar Cells. *Sustain. Energy Fuels* **2019**. https://doi.org/10.1039/c9se00493a.

(14) Reese, M. O.; Gevorgyan, S. A.; Jørgensen, M.; Bundgaard, E.; Kurtz, S. R.; Ginley, D. S.; Olson, D. C.; Lloyd, M. T.; Morvillo, P.; Katz, E. A.; Elschner, A.; Haillant, O.; Currier, T. R.; Shrotriya, V.; Hermenau, M.; Riede, M.; Kirov, K. R.; Trimmel, G.; Rath, T.; Inganäs, O.; Zhang, F.; Andersson, M.; Tvingstedt, K.; Lira-Cantu, M.; Laird, D.; McGuiness, C.; Gowrisanker, S.; Pannone, M.; Xiao, M.; Hauch, J.; Steim, R.; Delongchamp, D. M.; Rösch, R.; Hoppe, H.; Espinosa, N.; Urbina, A.; Yaman-Uzunoglu, G.; Bonekamp, J. B.; Van Breemen, A. J. J. M.; Girotto, C.; Voroshazi, E.; Krebs, F. C. Consensus Stability Testing Protocols for Organic Photovoltaic Materials and Devices. *Sol. Energy Mater. Sol. Cells* **2011**. https://doi.org/10.1016/j.solmat.2011.01.036.

(15) Khenkin, M. V.; Katz, E. A.; Abate, A.; Bardizza, G.; Berry, J. J.; Brabec, C.; Brunetti, F.; Bulović, V.; Burlingame, Q.; Di Carlo, A.; Cheacharoen, R.; Cheng, Y. B.; Colsmann, A.; Cros, S.; Domanski, K.; Dusza, M.; Fell, C. J.; Forrest, S. R.; Galagan, Y.; Di Girolamo, D.; Grätzel, M.; Hagfeldt, A.; von Hauff, E.; Hoppe, H.; Kettle, J.; Köbler, H.; Leite, M. S.; Liu, S. (Frank); Loo, Y. L.; Luther, J. M.; Ma, C. Q.; Madsen, M.; Manceau, M.; Matheron, M.; McGehee, M.; Meitzner, R.; Nazeeruddin, M. K.; Nogueira, A. F.; Odabaşı, Ç.; Osherov, A.; Park, N. G.; Reese, M. O.; De Rossi, F.; Saliba, M.; Schubert, U. S.; Snaith, H. J.; Stranks, S. D.; Tress, W.; Troshin, P. A.; Turkovic, V.; Veenstra, S.; Visoly-Fisher, I.; Walsh, A.; Watson, T.; Xie, H.; Yıldırım, R.; Zakeeruddin, S. M.; Zhu, K.; Lira-Cantu, M. Consensus Statement for Stability Assessment and Reporting for Perovskite Photovoltaics Based on ISOS Procedures. *Nat. Energy* **2020**. https://doi.org/10.1038/s41560-019-0529-5.

(16) Nie, W.; Blancon, J. C.; Neukirch, A. J.; Appavoo, K.; Tsai, H.; Chhowalla, M.; Alam, M. A.; Sfeir, M. Y.; Katan, C.; Even, J.; Tretiak, S.; Crochet, J. J.; Gupta, G.; Mohite, A. D. Light-Activated Photocurrent Degradation and Self-

Healing in Perovskite Solar Cells. *Nat. Commun.* **2016**. https://doi.org/10.1038/ncomms11574.

(17) Domanski, K.; Roose, B.; Matsui, T.; Saliba, M.; Turren-Cruz, S. H.; Correa-Baena, J. P.; Carmona, C. R.; Richardson, G.; Foster, J. M.; De Angelis, F.; Ball, J. M.; Petrozza, A.; Mine, N.; Nazeeruddin, M. K.; Tress, W.; Grätzel, M.; Steiner, U.; Hagfeldt, A.; Abate, A. Migration of Cations Induces Reversible Performance Losses over Day/Night Cycling in Perovskite Solar Cells. *Energy Environ. Sci.* **2017**. https://doi.org/10.1039/c6ee03352k.

(18) Ceratti, D. R.; Rakita, Y.; Cremonesi, L.; Tenne, R.; Kalchenko, V.; Elbaum, M.; Oron, D.; Potenza, M. A. C.; Hodes, G.; Cahen, D. Self-Healing Inside APbBr3 Halide Perovskite Crystals. *Adv. Mater.* **2018**. https://doi.org/10.1002/adma.201706273.

(19) Khenkin, M. V.; Anoop, K. M.; Visoly-Fisher, I.; Kolusheva, S.; Galagan, Y.; Di Giacomo, F.; Vukovic, O.; Patil, B. R.; Sherafatipour, G.; Turkovic, V.; Rubahn, H. G.; Madsen, M.; Mazanik, A. V.; Katz, E. A. Dynamics of Photoinduced Degradation of Perovskite Photovoltaics: From Reversible to Irreversible Processes. *ACS Appl. Energy Mater.* **2018**. https://doi.org/10.1021/acsaem.7b00256.

(20) Yadav, P.; Prochowicz, D.; Alharbi, E. A.; Zakeeruddin, S. M.; Grätzel, M. Intrinsic and Interfacial Kinetics of Perovskite Solar Cells under Photo and Bias-Induced Degradation and Recovery. *J. Mater. Chem. C* **2017**, *5* (31), 7799–7805. https://doi.org/10.1039/c7tc02652h.

(21) Mahapatra, A.; Parikh, N.; Kumar, P.; Kumar, M.; Prochowicz, D.; Kalam, A.; Tavakoli, M. M.; Yadav, P. Changes in the Electrical Characteristics of Perovskite Solar Cells with Aging Time. *Molecules* **2020**, *25* (10), 2299. https://doi.org/10.3390/molecules25102299.

(22) Jeong, K.; Byeon, J.; Jang, J.; Ahn, N.; Choi, M. Pulsatile Therapy for Perovskite Solar Cells. **2020**.

(23) Manor, A.; Katz, E. A.; Tromholt, T.; Krebs, F. C. Electrical and Photo-Induced Degradation of ZnO Layers in Organic Photovoltaics. *Adv. Energy Mater.* **2011**. https://doi.org/10.1002/aenm.201100227.

(24) Manor, A.; Katz, E. A.; Tromholt, T.; Krebs, F. C. Enhancing Functionality of ZnO Hole Blocking Layer in Organic Photovoltaics. *Sol. Energy Mater. Sol. Cells* **2012**, *98*, 491–493. https://doi.org/10.1016/j.solmat.2011.11.026.

(25) Głowienka, D.; Zhang, D.; Di Giacomo, F.; Najafi, M.; Veenstra, S.; Szmytkowski, J.; Galagan, Y. Role of Surface Recombination in Perovskite Solar Cells at the Interface of HTL/CH3NH3PbI3. *Nano Energy* **2020**. https://doi.org/10.1016/j.nanoen.2019.104186.

(26) Lopez-Varo, P.; Jiménez-Tejada, J. A.; García-Rosell, M.; Ravishankar, S.; Garcia-Belmonte, G.; Bisquert, J.; Almora, O. Device Physics of Hybrid Perovskite Solar Cells: Theory and Experiment. *Advanced Energy Materials*. 2018. https://doi.org/10.1002/aenm.201702772.

(27) Khenkin, M. V.; Anoop, K. M.; Katz, E. A.; Visoly-Fisher, I. Bias-Dependent Degradation of Various Solar Cells: Lessons for Stability of Perovskite Photovoltaics. *Energy and Environmental Science*. Royal Society of Chemistry February 1, 2019, pp 550–558. https://doi.org/10.1039/c8ee03475c.

(28) Anoop, K. M.; Khenkin, M. V.; Di Giacomo, F.; Galagan, Y.; Rahmany, S.; Etgar, L.; Katz, E. A.; Visoly-Fisher, I. Bias-Dependent Stability of Perovskite Solar Cells Studied Using Natural and Concentrated Sunlight. *Sol. RRL* **2020**. https://doi.org/10.1002/solr.201900335.

(29) Holzhey, P.; Yadav, P.; Turren-Cruz, S. H.; Ummadisingu, A.; Grätzel, M.; Hagfeldt, A.; Saliba, M. A Chain Is as Strong as Its Weakest Link – Stability Study of MAPbI3 under Light and Temperature. *Mater. Today* **2019**, *29*, 10–19. https://doi.org/10.1016/j.mattod.2018.10.017.

(30) Gottesman, R.; Lopez-Varo, P.; Gouda, L.; Jimenez-Tejada, J. A.; Hu, J.; Tirosh, S.; Zaban, A.; Bisquert, J. Dynamic Phenomena at Perovskite/Electron-Selective Contact Interface as Interpreted from Photovoltage Decays. *Chem* **2016**. https://doi.org/10.1016/j.chempr.2016.10.002.

(31) Zarazua, I.; Bisquert, J.; Garcia-Belmonte, G. Light-Induced Space-Charge Accumulation Zone as Photovoltaic Mechanism in Perovskite Solar Cells. **2016**. https://doi.org/10.1021/acs.jpclett.5b02810.

(32) Peng, J.; Chen, Y.; Zheng, K.; Pullerits, T.; Liang, Z. Insights into Charge Carrier Dynamics in Organo-Metal Halide Perovskites: From Neat Films to Solar Cells. *Chemical Society Reviews*. 2017. https://doi.org/10.1039/c6cs00942e.

(33) Berger, T.; Sterrer, M.; Diwald, O.; Knözinger, E.; Panayotov, D.; Thompson, T. L.; Yates, J. T. Light-Induced Charge Separation in Anatase TiO 2 Particles. *J. Phys. Chem. B* **2005**. https://doi.org/10.1021/jp0404293.

(34) Wilken, S.; Parisi, J.; Borchert, H. Role of Oxygen Adsorption in Nanocrystalline ZnO Interfacial Layers for Polymer-Fullerene Bulk Heterojunction Solar Cells. *J. Phys. Chem. C* **2014**. https://doi.org/10.1021/jp506641m.

(35) Trost, S.; Zilberberg, K.; Behrendt, A.; Polywka, A.; Görrn, P.; Reckers, P.; Maibach, J.; Mayer, T.; Riedl, T. Overcoming the "Light-Soaking" Issue in Inverted Organic Solar Cells by the Use of Al:Zno Electron Extraction Layers. *Adv. Energy Mater.* **2013**. https://doi.org/10.1002/aenm.201300402.

(36) Mirsafaei, M.; Jensen, P. B.; Ahmadpour, M.; Lakhotiya, H.; Hansen, J. L.; Julsgaard, B.; Rubahn, H. G.; Lazzari, R.; Witkowski, N.; Balling, P.; Madsen, M. Sputter-Deposited Titanium Oxide Layers as Efficient Electron Selective Contacts in Organic Photovoltaic Devices. *ACS Appl. Energy Mater.* **2020**. https://doi.org/10.1021/acsaem.9b01454.

(37) Domanski, K.; Correa-Baena, J. P.; Mine, N.; Nazeeruddin, M. K.; Abate, A.; Saliba, M.; Tress, W.; Hagfeldt, A.; Grätzel, M. Not All That Glitters Is Gold: Metal-Migration-Induced Degradation in Perovskite Solar Cells. *ACS Nano* **2016**. https://doi.org/10.1021/acsnano.6b02613.

(38) Li, Z.; Xiao, C.; Yang, Y.; Harvey, S. P.; Kim, D. H.; Christians, J. A.; Yang, M.; Schulz, P.; Nanayakkara, S. U.; Jiang, C. S.; Luther, J. M.; Berry, J. J.; Beard, M. C.; Al-Jassim, M. M.; Zhu, K. Extrinsic Ion Migration in Perovskite Solar Cells. *Energy Environ. Sci.* **2017**. https://doi.org/10.1039/c7ee00358g.

(39) Zoller, F.; Böhm, D.; Bein, T.; Fattakhova-Rohlfing, D. Tin Oxide Based Nanomaterials and Their Application as Anodes in Lithium-Ion Batteries and Beyond. *ChemSusChem*. 2019. https://doi.org/10.1002/cssc.201901487.

(40) Prakash, K.; Senthil Kumar, P.; Pandiaraj, S.; Saravanakumar, K.; Karuthapandian, S. Controllable Synthesis of SnO2 Photocatalyst with Superior Photocatalytic Activity for the Degradation of Methylene Blue Dye Solution. *J. Exp. Nanosci.* **2016**. https://doi.org/10.1080/17458080.2016.1188222.

(41) Aslam, M.; Qamar, M. T.; Ali, S.; Rehman, A. U.; Soomro, M. T.; Ahmed, I.; Ismail, I. M. I.; Hameed, A. Evaluation of SnO2 for Sunlight Photocatalytic Decontamination of Water. *J. Environ. Manage.* **2018**. https://doi.org/10.1016/j.jenvman.2018.04.042.

(42) Yang, L.; Yang, Y.; Liu, T.; Ma, X.; Lee, S. W.; Wang, Y. Oxygen Vacancies Confined in SnO2 Nanoparticles for Glorious Photocatalytic Activities from the UV, Visible to near-Infrared Region. *New J. Chem.* **2018**. https://doi.org/10.1039/c8nj00668g.

(43) Kim, J.-H.; Lee, I.; Kim, T.-S.; Rolston, N.; Watson, B. L.; Dauskardt, R. H. Understanding Mechanical Behavior and Reliability of Organic Electronic Materials. *MRS Bull.* **2017**, *42* (02), 115–123. https://doi.org/10.1557/mrs.2017.3.

(44) Jacobs, D. A.; Wu, Y.; Shen, H.; Barugkin, C.; Beck, F. J.; White, T. P.; Weber, K.; Catchpole, K. R. Hysteresis Phenomena in Perovskite Solar Cells: The Many and Varied Effects of Ionic Accumulation. *Phys. Chem. Chem. Phys.* **2017**, *19* (4), 3094–3103. https://doi.org/10.1039/c6cp06989d.

(45) Głowienka, D.; Szmytkowski, J. Numerical Modeling of Exciton Impact in Two Crystalographic Phases of the Organo-Lead Halide Perovskite (CH 3 NH 3 PbI 3) Solar Cell. *Semicond. Sci. Technol.* **2019**. https://doi.org/10.1088/1361-6641/aafeef.

(46) Sherkar, T. S.; Momblona, C.; Gil-Escrig, L.; Ávila, J.; Sessolo, M.; Bolink, H. J.; Koster, L. J. A. Recombination in Perovskite Solar Cells: Significance of Grain Boundaries, Interface Traps, and Defect Ions. *ACS Energy Lett.* **2017**. https://doi.org/10.1021/acsenergylett.7b00236.

(47) Jiang, Q.; Zhang, L.; Wang, H.; Yang, X.; Meng, J.; Liu, H.; Yin, Z.; Wu, J.; Zhang, X.; You, J. Enhanced Electron Extraction Using SnO2 for High-Efficiency Planar-Structure HC(NH2)2 PbI3-Based Perovskite Solar Cells. *Nat.*

Energy **2017**. https://doi.org/10.1038/nenergy.2016.177.

(48) Nagasawa, M.; Shionoya, S.; Makishima, S. Electron Effective Mass of SnO2. *J. Phys. Soc. Japan* **1965**. https://doi.org/10.1143/JPSJ.20.1093.

(49) Manzoor, S.; Häusele, J.; Bush, K. A.; Palmstrom, A. F.; Carpenter, J.; Yu, Z. J.; Bent, S. F.; Mcgehee, M. D.; Holman, Z. C. Optical Modeling of Wide-Bandgap Perovskite and Perovskite/Silicon Tandem Solar Cells Using Complex Refractive Indices for Arbitrary-Bandgap Perovskite Absorbers. *Opt. Express* **2018**. https://doi.org/10.1364/oe.26.027441.

(50) Brivio, F.; Butler, K. T.; Walsh, A.; Van Schilfgaarde, M. Relativistic Quasiparticle Self-Consistent Electronic Structure of Hybrid Halide Perovskite Photovoltaic Absorbers. *Phys. Rev. B - Condens. Matter Mater. Phys.* **2014**. https://doi.org/10.1103/PhysRevB.89.155204.

(51) Park, S.; Heo, J. H.; Cheon, C. H.; Kim, H.; Im, S. H.; Son, H. J. A [2,2]Paracyclophane Triarylamine-Based Hole-Transporting Material for High Performance Perovskite Solar Cells. *J. Mater. Chem. A* **2015**. https://doi.org/10.1039/c5ta08417b.

(52) Filipič, M.; Löper, P.; Niesen, B.; De Wolf, S.; Krč, J.; Ballif, C.; Topič, M. CH_3NH_3PbI_3 Perovskite / Silicon Tandem Solar Cells: Characterization Based Optical Simulations. *Opt. Express* **2015**. https://doi.org/10.1364/oe.23.00a263.

(53) Cielecki, P. P. P.; Sobolewska, E. K.; Kostiuočenko, O.; Leißner, T.; Tamulevičius, T.; Tamulevičius, S.; Rubahn, H. G.; Adam, J.; Fiutowski, J. Plasmon–Organic Fiber Interactions in Diamond-like Carbon Coated Nanostructured Gold Films. *Opt. Commun.* **2017**. https://doi.org/10.1016/j.optcom.2017.06.064.

(54) Cielecki, P. P.; Adam, J.; Leißner, T.; Patil, B. R.; Madsen, M.; Rubahn, H. G.; Kjelstrup-Hansen, J.; Fiutowski, J. Photo-Induced Degradation Mechanisms in 4P-NPD Thin Films. *Org. Electron.* **2018**. https://doi.org/10.1016/j.orgel.2018.08.047.

(55) Cielecki, P. P.; Leißner, T.; Ahmadpour, M.; Madsen, M.; Rubahn, H. G.; Fiutowski, J.; Kjelstrup-Hansen, J. Photo-Induced and Electrical Degradation of Organic Field-Effect Transistors. *Org. Electron.* **2020**. https://doi.org/10.1016/j.orgel.2020.105717.